Atmos. Chem. Phys. Discuss., doi:10.5194/acp-2017-450, 2017
Manuscript under review for journal Atmos. Chem. Phys.
Discussion started: 19 May 2017

Atmospheric Chemistry and Physics Discussions

Unveiling aerosol-cloud interactions Part 1: Cloud contamination in satellite products enhances the aerosol indirect forcing estimate

Matthew W. Christensen[1,2], David Neubauer[3], Caroline Poulsen[1], Gareth Thomas[1], Greg McGarragh[2], Adam C. Povey[4], Simon Proud[2], and Roy G. Grainger[4]

[1]RAL Space, STFC Rutherford Appleton Laboratory, Harwell, OX11 0QX, United Kingdom
[2]Atmospheric, Oceanic and Planetary Physics, University of Oxford, Oxford, OX1 3PU, United Kingdom
[3]Institute for Atmospheric and Climate Science, ETH Zurich, Zurich, 8092, Switzerland
[4]National Centre for Earth Observation, University of Oxford, Oxford, OX1 3PU, United Kingdom

Correspondence to: Matthew Christensen (Matthew.Christensen@stfc.ac.uk)

Abstract. Increased concentrations of aerosol can enhance the albedo of warm low-level cloud. Accurately quantifying this relationship from space is challenging due in part to contamination of aerosol statistics near clouds. Aerosol retrievals near clouds can be influenced by stray cloud particles in areas assumed to be cloud-free, particle swelling by humidification, shadows and enhanced scattering into the aerosol field from (3D radiative transfer) clouds. To screen for this contamination we have developed a new Cloud-Aerosol Pairing Algorithm (CAPA) to link cloud observations to the nearest aerosol retrieval within the satellite image. The distance between each aerosol retrieval and nearest cloud is also computed in CAPA.

Results from two independent satellite imagers, the Advanced Along Track Scanning Radiometer (AATSR) and MODerate Resolution Imaging Spectroradiometer (MODIS) show a marked reduction in the strength of the intrinsic aerosol indirect forcing when selecting aerosol pairs that are located farther away from the clouds (-0.28 ± 0.26 W/m^2) compared to those including pairs that are within 15 km of the nearest cloud (-0.49 ± 0.18 W/m^2). The larger aerosol optical depths in closer proximity to cloud artificially enhance the relationship between aerosol loading, cloud albedo, and cloud fraction. These results suggest that previous satellite-based radiative forcing estimates represented in key climate reports may be exaggerated due to including retrieval artefacts in the aerosol located near clouds.

1 Introduction

Aerosols are hypothesised to cool the climate system due to their ability to enhance the reflection of clouds (Twomey, 1974; Albrecht, 1989), particularly ubiquitous warm phase clouds located in the boundary layer (Christensen et al., 2016a). The uncertainty attached to this cooling effect is considered to be very large (IPCC, 2013) in both satellite and general circulation model (GCM) estimates. The fundamental issues causing this large uncertainty stem from a myriad of challenges related to retrieval artefacts in satellite products (e.g. cloud contamination and 3D radiative effects) and missing processes in GCMs (e.g. parameterisation schemes to include effects of buffering from meteorology on aerosol-cloud interactions as discussed in Stevens and Feingold, 2009). Satellite observations suggest that the aerosol indirect radiative cooling effect is about half that

Atmos. Chem. Phys. Discuss., doi:10.5194/acp-2017-450, 2017
Manuscript under review for journal Atmos. Chem. Phys.
Discussion started: 19 May 2017

Atmospheric Chemistry and Physics Discussions

of GCM-based estimates. For future climate projections it is critical to close the satellite-GCM gap in the forcing estimate so we can understand to what extent anthropogenic aerosols may have cooled, and continue to cool, the climate system.

Despite the advances in satellite-based retrievals in recent decades, obtaining robust statistical relationships between aerosols and clouds remain difficult. The challenges are primarily related to the following issues: (1) an artificially high aerosol optical depth (AOD) retrieval due to the presence of undetected cloud in areas assumed to be cloud-free (cloud contamination) (Remer et al., 2005); (2) radiation scattered by clouds that illuminate the aerosol field and are not accounted for in the 1-D radiative transfer model in satellite retrievals causing erroneously high AOD retrievals (Varnái and Marshak, 2009), (3) humidification causing aerosols to swell near clouds thereby enhancing AOD without any increase in aerosol number concentration (Twohy et al., 2009), (4) the representativeness of non-collocated aerosol and cloud retrievals, (5) the suitability of AOD as a proxy for cloud condensation nuclei (CCN) (Stier, 2016), and (6) the difficulty in inferring causality from covariability.

Recent assessments characterising the near-cloud aerosol contamination effects were examined using spaceborne lidar (Várnai et al., 2013) and ground-based lidar (Ten Hoeve and Augustine, 2016) observations. In general, the MODerate Resolution Imaging Spectroradiometer (MODIS) aerosol products show enhanced aerosol optical depth and particle sizes several kilometres beyond the cloud edge (Várnai and Marshak, 2015). Evidence from selected Surface Radiation Budget Network (SURFRAD) observations reported in Ten Hoeve and Augustine (2016) suggest that near-cloud contamination in the satellite retrieval can enhance the aerosol effect on cloud cover fraction by approximately 40% (i.e. cloud cover fraction is larger for the same aerosol optical depth when cloud contaminated pixels are used in the analysis). In addition, the direct aerosol radiative effect (i.e. the increase in reflected radiation due to aerosol loading in clear-sky conditions) in satellite observations is significantly larger (Twohy et al., 2009). The extent to which these near-cloud aerosols influence the correlation-based statistics used as diagnostics for aerosol-cloud interactions in satellite observations is largely unknown at the global scale. The quantification of their impacts on the aerosol radiative forcing estimate is the goal of this study.

Besides contamination, attributing causal relationships between non-collocated cloud and aerosol retrievals is challenging. Current passive sensors don't retrieve aerosol and cloud simultaneously because the imager pixels are classified as being either "cloud" or "cloud-free." To solve the collocation problem a **pre-averaging** methodology is commonly used (e.g. Sekiguchi et al., 2003; Quaas et al., 2008; Lebsock et al., 2008; Grandey and Stier, 2010; Chen et al., 2014; Gryspeerdt et al., 2016; Christensen et al., 2016a). Typically, the aerosol and cloud properties are pre-averaged over broad regions as a means to encapsulate both retrieval types together within a (level-3 type) grid-box. The aerosol and cloud bins are typically constructed at a spatial scale of $1^\circ \times 1^\circ$ at daily time intervals. This method limits the number of sampling pairs to roughly 90 (for a three month period) from which to derive seasonal regression statistics. A disadvantage to using this data is, if the pre-averaged data is not properly screened during averaging, the aerosol-cloud relationships may contain satellite artefacts caused by humidification and 3D effects near cloud edges.

Another, less common method to collocate aerosols and clouds together is **data assimilation**. This process uses aerosol properties that are extracted from reanalysis products at the location of the observed cloud (Bellouin et al., 2013; Amiri-Farahani et al., 2016). However, aerosols assimilated into models may be strongly affected by wet deposition (Gryspeerdt

Atmos. Chem. Phys. Discuss., doi:10.5194/acp-2017-450, 2017
Manuscript under review for journal Atmos. Chem. Phys.
Discussion started: 19 May 2017

Atmospheric Chemistry and Physics Discussions

et al., 2015) and influence the strength of aerosol indirect effects from aerosols sampled in clear-sky regions using satellite-only products (Christensen et al., 2016a).

In this paper, we have developed a new collocation method, defined here as the high-resolution **Cloud-Aerosol Pairing Algorithm** (CAPA). In this method high-resolution pixel-scale cloud observations are paired to the nearest aerosol retrieval within the satellite image. These pairs are then aggregated over $1^\circ \times 1^\circ$ regions. This results in a significant boost to the total number of samples used in the regression statistics from about 90 (using $1^\circ \times 1^\circ$ pre-averaged daily statistics) to approximately 3×10^5 using CAPA. In addition, the distance between cloud-aerosol retrievals can be adjusted in CAPA as a means to screen for aerosols next to clouds. This method provides the ability to expose biases in the aerosol-cloud radiative forcing estimate due to contamination in near-cloud aerosols.

The manuscript is organised into the following format: satellite data sets and their corresponding retrieval algorithms are described in section 2, the procedure to compute aerosol indirect radiative forcing in section 3, CAPA is described in section 4, compositing techniques are described in section 5, the results using this approach are compared to the standard pre-averaging method as described in section 6, and the summary and discussion of this work and how it relates to our companion paper (Neubauer et al., 2017) is described in section 7.

2 Satellite Data

Two passive satellite sensors are used in this study. The Advanced Along Track Scanning Radiometer (AATSR) on Envisat is a dual-view instrument having a footprint resolution of about 1 km at the surface. The two views (satellite zenith angles at $\sim 55^\circ$ forward and nadir) offered by the instrument provide near-simultaneous (within 90 seconds) observations of the same location on the Earth. This provides the ability to separate the surface from the atmospheric signals in order to increase the accuracy of the 1-km aerosol retrieval (in version 4.01 the aerosol is reported at 1 km resolution) using the Optimal Retrieval of Aerosol and Cloud (ORAC) algorithm (Thomas et al., 2009). Cloud properties are also retrieved using the same inputs (e.g. the cloud mask, surface reflectance data over the ocean, basis for the optimal estimation scheme in the radiative transfer model, and thermodynamic profiles) as the aerosol retrieval algorithm. By using the same inputs for the ORAC forward model we achieve a high-degree of consistency between the aerosol and cloud products. This consistency is essential to constraining the complexity in attributing cause and effect in aerosol-cloud interaction studies. The ORAC algorithm for cloud is described in (Poulsen et al., 2012; Sus et al., 2017; McGarragh et al., 2017) and the high-resolution pixel-scale data is currently available through the European Space Agency (ESA) Climate Change Initiative (CCI). The pre-averaged gridded daily products (L3C) used in this study are also available via http://cci.esa.int.

Shortwave and longwave broadband radiative fluxes are obtained using the CC4CL (Community Cloud Retrieval for Climate) algorithm (Christensen et al., 2016b) which is based on ORAC. The code uses the BUGSrad radiative transfer model (Stephens et al., 2001) in conjunction with the input cloud and aerosol properties derived from ORAC. BUGSrad is based on the two-stream approximation and correlated-k distribution methods of atmospheric radiative transfer. It is applied to a single-column atmosphere for which the cloud and aerosol layers are assumed to be plane-parallel. Cloud and aerosol properties

Atmos. Chem. Phys. Discuss., doi:10.5194/acp-2017-450, 2017
Manuscript under review for journal Atmos. Chem. Phys.
Discussion started: 19 May 2017

Atmospheric Chemistry and Physics Discussions

retrieved using ORAC are ingested into BUGSrad to compute both shortwave and longwave radiative fluxes for the top and bottom of atmosphere. The algorithm uses 18 bands that span the electromagnetic spectrum to compute the broadband flux, 6 in the shortwave and 12 in the longwave. BUGSrad shows good agreement with CERES observations (Henderson et al., 2013) and has been used to assess the Earth's energy budget using CloudSat observations (Stephens et al., 2012).

The MODIS 1-km pixel-scale data is obtained from the Terra satellite. Terra was selected for comparison because it has a similar orbit and equator crossing time as Envisat (approximately 10:30 am local time). To obtain top of atmosphere (TOA) radiative fluxes from MODIS on Terra we ingest the standard collection 6 cloud (MOD06; Baum et al., 2012) and aerosol (MOD04; Levy et al., 2013) into the CC4CL radiative flux BUGSrad model. The ESA CCI projects evaluated several aerosol and cloud products, among them were the standard collection 6 MODIS aerosol and cloud products. ORAC was also applied to MODIS data (within Cloud_cci) and the MODIS-ORAC product was found to agree very well with the MODIS standard products (Hollmann, 2017).

This analysis uses ten years of AATSR observations spanning from 2002 to 2012. Pixels are screened to include only low-level (cloud top pressure greater than 500 hPa) liquid phase (cloud top temperature greater than 273 K) maritime clouds. Due to limitations in data storage we are only able process three months (June, July, and August; JJA) using high-resolution MODIS-ORAC (broadband fluxes derived using standard MODIS products) Terra retrievals for comparison.

3 Aerosol Indirect Forcing Calculation

Computation of the aerosol indirect radiative forcing estimate is based on a top-down approach in which a system-wide variable, the cloud radiative effect (CRE), is used to compute the radiative forcing as a function of the aerosol loading. This reduces the number of free-parameters to just a few (e.g. cloud fraction, cloud albedo, and aerosol index) in which the observational uncertainties are better known (Feingold et al., 2016) compared to other quantities that are difficult to retrieve from passive satellite measurements (e.g. droplet number concentration, cloud condensation nuclei, cloud thickness). Even active sensors (e.g. CloudSat) have difficulty retrieving these quantities with lower uncertainty and have much poorer spatial coverage compared to passive sensing instruments. The derivation of the shortwave component of aerosol indirect forcing at the top of the atmosphere is the same as that used in Chen et al. (2014) and is derived from the cloud radiative effect equation written here as

$$F_{\mathrm{CRE}} = F_{\mathrm{clr}} - F_{\mathrm{obs}} \tag{1}$$

where F_{clr} is the clear sky net radiative flux (i.e., $F_{\mathrm{clr}} = F^{\uparrow}_{\mathrm{clr}} - F^{\downarrow}_{\mathrm{clr}}$, arrows denote the upwelling and downwelling fluxes, respectively) for atmospheric columns containing no clouds and F_{obs} is the net flux that is observed for all-sky conditions (excluding ice clouds here) which, assuming a relatively dark ocean surface can be decomposed into

$$F_{\mathrm{obs}} = (1 - c_{\mathrm{f}})F_{\mathrm{clr}} + c_{\mathrm{f}}F_{\mathrm{cld}} \tag{2}$$

where F_{cld} is the component of the radiative flux contributed by clouds and c_{f} is the cloud cover fraction over the observed area. Combining equations (1) and (2) and considering the shortwave component of the upwelling fluxes the cloud radiative

Atmos. Chem. Phys. Discuss., doi:10.5194/acp-2017-450, 2017
Manuscript under review for journal Atmos. Chem. Phys.
Discussion started: 19 May 2017

Atmospheric Chemistry and Physics Discussions

effect becomes

$$F_{\mathrm{CRE}} = c_{\mathrm{f}}(A_{\mathrm{clr}} - A_{\mathrm{cld}})F^{\downarrow} \tag{3}$$

where A_{clr} is the clear-sky albedo and A_{cld} is the albedo of the cloud. Taking the derivative of equation (3) with respect to the aerosol index (AI) gives the TOA aerosol indirect radiative effect

$$\frac{dF^{\mathrm{sw}}_{\mathrm{CRE}}}{d\ln AI} = \left(\overline{c_{\mathrm{m}}}\left[\frac{dA_{\mathrm{clr}}}{d\ln AI} - \frac{dA_{\mathrm{cld}}}{d\ln AI}\right] + \overline{(A_{\mathrm{clr}} - A_{\mathrm{cld}})}\frac{dc_{\mathrm{f}}}{d\ln AI}\right)F^{\downarrow} \tag{4}$$

where $\overline{c_{\mathrm{m}}}$ is the climatology of low-level clouds having cloud top pressure greater than 500 hPa and composed of liquid phase droplets over ocean regions, the derivative terms represent the change in clear-sky and cloudy-sky albedo as a function of aerosol index, $F^{\downarrow}$ is the annual mean incoming solar radiation at the top of the atmosphere (computed using the method outlined in Coakley, 1979). The first term on the right-hand side of equation (4) is called the intrinsic aerosol effect and represents the impact of aerosol on changes in cloud albedo. The second term is the extrinsic effect which represents the impact of aerosol on cloud fraction. We use aerosol index ($AI = \tau_{\mathrm{a}} \times \mathring{A}$, where τ_{a} is the aerosol optical depth at 550 nm and $\mathring{A}$ is the Ångström exponent derived from the optical depths at 550 nm and 869 nm) because it has been shown to serve as a better indicator of the column cloud condensation nuclei (Nakajima et al., 2001) compared to aerosol optical depth.

Finally, the aerosol indirect forcing estimate is obtained by multiplying equation (4) by an amount of aerosol attributable to anthropogenic activities as determined by MACC-II reanalysis data (i.e., $\Delta\tau_{\mathrm{a}} = \ln(\tau_{\mathrm{a}}) - \ln(\tau_{\mathrm{a}} - \tau_{\mathrm{anth}}) = \ln\left(\frac{1}{1-F_{\mathrm{anth}}}\right)$, where τ_{anth} is the aerosol optical depth attributed to anthropogenic activities). MACC-II is a satellite-model hybrid dataset that utilises the state-of-the-art ECMWF-IFS (Integrated Forecast System) aerosol transport model along with a surface emissions inventory and assimilated MODIS data to provide aerosol optical depth for a variety of species including dust, organic carbon, sea-salt, black carbon, and sulphate (e.g. see Morcrette et al. (2009) and Benedetti et al. (2009) for details). Global distributions of the anthropogenic aerosol fraction are provided in Chen et al. (2014) and Bellouin et al. (2013); the global oceanic mean value is about 21%.

4 Cloud-Aerosol Pairing Algorithm (CAPA)

The basic approach of CAPA is to pair each cloud observation to the nearest aerosol retrieval. This process is performed within the satellite image (the swath width is 2330 km for MODIS and 512 km for AATSR). Distances, using Euclidian geometry in pixel-coordinates, are computed between each cloud pixel and all possible aerosol retrievals. Given the large number of pixels within the swath this task is computationally demanding if proper screening is not carried out initially. To decrease computation time and the number of possible pairs (for a given cloud observation), the satellite image is divided into sections and pixels are grouped together (typically 250×250 square regions). This step eliminates aerosol-cloud pairs at distances greater than approximately 150 km (for 1-km pixel-scale data), but potential pairs beyond this length-scale are probably less relevant since the cloud-aerosol interaction is less likely to be influenced by the same airmass (Anderson et al., 2003).

In the next step the cloud fraction is computed (using the satellite retrieval cloud mask) as a metric to determine the appropriate search algorithm to use for the given subsection of the satellite granule. If the cloud fraction is high ($c_{\mathrm{f}} > 50\%$) then fewer

Atmos. Chem. Phys. Discuss., doi:10.5194/acp-2017-450, 2017
Manuscript under review for journal Atmos. Chem. Phys.
Discussion started: 19 May 2017

Atmospheric Chemistry and Physics Discussions

aerosol retrievals exist and the distance between each cloud pixel and all aerosol pixels is computed simultaneously via brute force within that region of the satellite orbit. However, if the cloud fraction is low ($c_{\mathrm{f}} < 50\%$) the number of aerosol targets will be large and the former approach will run much slower. In this case the pixels that are adjacent to the cloud observation are searched first (as there is a relatively high probability an aerosol is located in an adjacent pixel). If an aerosol retrieval is not found in the adjacent pixels this step is repeated, again, until an aerosol target is found. By using both search algorithms together (based on cloud fraction) the computation speed decreases by more than 50% compared to running the retrieval in brute-force mode alone. The CAPA run time is approximately 2-6 minutes using a single core Intel/AMD at ~ 3 GHz processor for a typical MODIS granule that contains 2.5 million 1-km pixels.

The results of CAPA are applied to part of an AATSR orbit and displayed in Figure 1. The image shows a belt of clouds across the middle of the granule with aerosols retrieved on both sides (Figure 1b). The cloud-belt is approximately 300 km wide (Figure 1c). Aerosols in the lower half of the image have lower optical depths and tend to be located at greater distances to the nearest cloud (green pixels). Whereas the aerosols in the upper half of the image are retrieved mostly in a broken cloud field in which the aerosols are located close to the clouds (red pixels). The aerosol retrievals have a "blocky" appearance because the standard level-2 aerosol products from MODIS (MOD04) and AATSR (V4.02) are averaged over larger 10 km^2 pixels. To match the cloud and aerosol products together (on the same imager pixel grid) we resample these aerosol products at 1 km resolution so that aerosol-cloud pairs can be constructed.

Aerosol statistics are examined as a function of distance to the nearest cloud in Figure 2. The observations are comprised of three months (JJA in 2008) of data collected across four different $10^\circ \times 10^\circ$ regions (off the coasts of California, Peru, Azores, and Namibia). In every region, the mean aerosol optical depth and particle size (inferred from the Ångström exponent) increase as the observations are closer in distance to the nearest cloud. In agreement with previous studies we find that about half of all clear-sky columns occur within $4-5$ km of the low-level cloud (Várnai and Marshak, 2012). As a consequence, near-cloud aerosols in pre-averaged aerosol datasets would provide substantial weight (and contamination) to the aerosol statistics.

Despite efforts to limit contamination in standard MODIS collection 6 retrievals - threshold values for the darkest and brightest 25% of pixels in each cluster (Remer et al., 2005) are applied - artificially large aerosol optical depths remain in the MODIS observed pixels near cloud edges, due primarily to 3D effects (Varnái and Marshak, 2009). Currently, no effort is made to remove near-cloud pixels from the AATSR ORAC gridded-products. This is evident from the faster and less pronounced decrease in aerosol optical depth and Ångström exponent with distance from the nearest cloud in the MODIS product. The contamination effect is greatly reduced at distances greater than 15 km, where the aerosol optical properties tend to be fairly constant beyond this length-scale. Similarly, Varnái and Marshak (2009) also noted that beyond 15 km contamination effects were minimised in MODIS data. We therefore use the 15 km length-scale to form the basis of the data compositing in this study.

Atmos. Chem. Phys. Discuss., doi:10.5194/acp-2017-450, 2017
Manuscript under review for journal Atmos. Chem. Phys.
Discussion started: 19 May 2017

Atmospheric Chemistry and Physics Discussions

5 Data Stratification

Results are based on four distinct composites of the data as listed in Table 1. Each composite contains aerosol and cloud pairs which are aggregated into $1^\circ \times 1^\circ$ regions so that regression statistics can be computed on the basis of the linear least-squares slope between the cloud albedo and the aerosol index. Two distinct methodological frameworks are used, 1) the high-resolution CAPA and 2) the low-resolution pre-averaging methods.

CAPA is run using two distinct length-scales: 1) clouds are paired based on the nearest located aerosol (CAPA-L2) and based on the nearest aerosol that is located at least 15 km away from any other cloud (CAPA-L2_15km). The median distance between aerosol and cloud pairs from these two composites is 8.2 and 27.1 km, respectively thereby providing the ability to screen for aerosol next to cloud. Another advantage of CAPA is that it retains individual L2 pixels, i.e. full-resolution data, for quantifying aerosol-cloud relationships over each 1° grid-box allowing for more of the aerosol field to be sampled, thus providing more degrees of freedom which to derive seasonal statistics. For example, the average number of high-resolution samples going into a typical 1° region over a three month period is approximately 3.0×10^5, although the actual number of degrees of freedom is much smaller (each region provides on average about 10 degrees of freedom per day providing roughly 1000 over a three month period) owing to oversampling the same aerosol used to make cloud-aerosol pairs. Nevertheless, the typical number of samples in the CAPA composites far exceed those that can be achieved using the standard pre-averaged products (PRE_AVG-L3 and PRE_AVG-L3_Corr.) where at most they provide 90 samples (providing one aerosol-cloud pair sample per-day for a given grid-box) in a three month period. As pointed out later, the nearly one full order of magnitude fewer unique aerosol-cloud pairs in the PRE_AVG-L3 composite results in a larger 1-σ regression error estimate.

6 Results

Aerosol-cloud relationships are examined using the CAPA and pre-average methods at a variety of spatiotemporal scales. To determine the suitability of this new method the results are displayed at the regional-scale ($10^\circ \times 10^\circ$) in selected locations with predominately low-level clouds (i.e. off the coasts of California, Peru, Azores, and Namibia) and at the global-scale.

6.1 Global distributions

The intrinsic aerosol-cloud effect is predominately influenced by the change in cloud albedo as a function of the aerosol index (i.e. $\frac{dA_{cld}}{d\ln AI}$). The regression is quantified using a range of temporal averaging periods using AATSR observations in Figure 3. As more years of observations are included in the regression the global distribution becomes less noisy (as represented by a decrease in the standard deviation from $\sigma = 0.05$ to 0.02 for the PRE_AVG-L3 composite). The globally averaged standard error on the regression slope essentially decreases as the sample size of cloud-aerosol pairs increases. Although, beyond 5 years the differences in the intrinsic effect between consecutive years become statistically insignificant. We conclude that 10 years of AATSR observations are more than adequate to construct these diagnostics. Regarding MODIS, we acknowledge that

Atmos. Chem. Phys. Discuss., doi:10.5194/acp-2017-450, 2017
Manuscript under review for journal Atmos. Chem. Phys.
Discussion started: 19 May 2017

Atmospheric Chemistry and Physics Discussions

the limited 3-month time period may bias the standard error of the regression slope. Therefore, it is used primarily to test the new CAPA method.

Figure 4 shows the global distribution of the observed intrinsic aerosol indirect forcing estimate using AATSR observations. Consistent with Chen et al. (2014), larger values are observed in the Northern Hemisphere in accordance with the larger fractions of anthropogenic aerosol and maritime low-level clouds. Another, more notable, result displayed in Figures 3 & 4 is the substantial decrease in the strength of the forcing when using the CAPA algorithm to screen for aerosols in the vicinity of clouds (i.e. between CAPA-L2_15km and the CAPA-L2 and PRE_AVG-L3 composites). Because all three composites use the same cloud fraction and anthropogenic aerosol fraction climatologies the differences are primarily due to the weaker cloud albedo sensitivities as inferred from equation (4) and displayed in Figure 3.

6.2 Regression Tests at Regional-Scales

To understand why the cloud albedo effect sensitivity is weaker when screening for aerosols close to clouds we examine the diagnostics in several regions across the globe. Figure 5 shows the mean cloud albedo plotted as a function of the aerosol index for the California region. The linear regression slope between cloud albedo and AI is stronger when the clouds are paired to contaminated aerosols located within 15 km from another cloud. The cloud albedo also tends to increase monotonically as a function of AI until reaching a value of about 0.25 in the CAPA-L2 composite. Beyond this value cloud albedo increases at a slower rate because the clouds become less susceptible in a more polluted atmosphere. By contrast, when pairing the same clouds to aerosols that are located at least 15 km from another cloud the aerosol index values shift to smaller values and the slope between cloud albedo and AI decreases. Similar responses are also found in thicker clouds that are less "susceptible" (Platnick and Twomey, 1994) to aerosol perturbations (red points in Figure 5 and Figure 6) as well as in three other regions (Figure 6). These results suggest that aerosols located in the vicinity of clouds may be more likely to contaminate and inflate the statistical relationships between cloud and aerosol properties.

6.3 Aerosol-Cloud Radiative Forcing Estimates

Intrinsic aerosol-cloud radiative forcing estimates are provided for each composite in Figure 7. The independently derived estimates from AATSR and MODIS agree with each other and with the reported value in MODIS afternoon-train observations in Chen et al. (2014) to within 0.1 W m^{-2}. This relatively good agreement occurs despite the use of different temporal averaging periods. Comparisons are also made between composites that attempt to remove aerosol in the vicinity of clouds. We find that when no aerosol screening takes place in the pre-averaged gridded (PRE_AVG-L3) and high-resolution cloud-paring data sets (CAPA-L2) the forcing estimates are nearly two-times larger than the composites that screen for aerosol near cloud. This is due to the weaker relationship between cloud albedo and AI sensitivity for the aerosols selected farther away from clouds (CAPA-L2_15km).

Extrinsic aerosol-cloud radiative forcing estimates are shown in Figure 9. In agreement with previous studies (e.g. Quaas et al., 2010; Chand et al., 2012; Grandey et al., 2013; Gryspeerdt et al., 2014) we find the c_f-AI relationship is strongly positive in most locations thereby producing a very strong radiative forcing (Figure 8). However, after reconstructing the pre-

Atmos. Chem. Phys. Discuss., doi:10.5194/acp-2017-450, 2017
Manuscript under review for journal Atmos. Chem. Phys.
Discussion started: 19 May 2017

Atmospheric Chemistry and Physics Discussions

averaged aerosol data set based on screening out the aerosols close to clouds (PRE_AVG_Corr. composite) this process results in a decreased extrinsic aerosol indirect forcing estimate by approximately 70%. This result agrees with the ground-based SURFRAD observations reported in Ten Hoeve and Augustine (2016) in which the removal of aerosols in the vicinity of clouds decreased the strength of the cloud fraction aerosol loading relationship. Furthermore, because cloud fraction co-varies with relative humidity this estimate is still likely to be over estimated and could be further mitigated through the use of cloud droplet number concentration (Gryspeerdt et al., 2016).

Since there are numerous studies using pre-averaged level-3 type aerosol products we have tested how these products can be corrected. Here, we have reconstructed the pre-averaged aerosol product at first through the removal of near-cloud aerosols in the standard AATSR and MODIS data. Interestingly, similar forcing estimates are obtained when the cloud-contaminated aerosol is screened and pre-averaged over $1^\circ \times 1^\circ$ regions compared to the high-resolution aerosol-screened CAPA-L2_15km data. However, the CAPA methods produce smaller 1-σ standard error regression uncertainties (by up to 15%) due to including a larger number of unique cloud-aerosol sampling pairs over each 1° region. This result suggests that similar estimates can be obtained if stricter screening of the aerosols are carried out first in the pre-averaged products.

Overall, the intrinsic radiative forcing estimate of -0.49 ± 0.18 agrees with the values reported in previous satellite-based studies (e.g., Sekiguchi et al. (2003); Quaas et al. (2008); Lebsock et al. (2008); Bellouin et al. (2013); Chen et al. (2014); Christensen et al. (2016a)). However, when the aerosols are removed from the vicinity of clouds these methods produce radiative forcing estimates that are smaller by about 40%. In addition, the extrinsic forcing decreases by 70%. These results suggest that satellite-based estimates represented in key climate reports (e.g. see the IPCC, 2013) may be exaggerated due to retrieval artefacts in the aerosol properties next to clouds. A summary of the estimates derived for oceanic regions are reported in Table 2.

7 Conclusions

Two independent satellite instruments, AATSR on Envisat and MODIS on Terra, were used in this study to test a new cloud-aerosol pairing algorithm to compute aerosol indirect forcing estimates for warm oceanic maritime clouds. Cloud-aerosol pairs formed at the pixel-scale resolution of the satellite imager using CAPA can provide a larger sample size from which to compute correlation statistics between cloud albedo and aerosol index. The effect of the larger sample size effectively decreases the standard error of the regression slope thereby providing higher confidence in the new radiative forcing estimates.

The scheme was also developed to determine the extent to which artefacts in aerosol retrievals located in the vicinity of clouds affect aerosol-cloud relationships in spaceborne satellite observations. By removing aerosols located within 15 km of the nearest cloud, both the cloud albedo effect (intrinsic) and cloud fraction effect (extrinsic) forcing decreased by 40% and 70%, respectively. These new estimates suggest that aerosol effects on the radiative properties of clouds are even smaller than previously demonstrated from satellite-based studies. This new methodology therefore further widens the gap between satellite and the very strong forcing estimates derived using GCMs.

Extension of this method in comparison with GCMs is explored in the companion paper of Neubauer et al. (2017). Furthermore, this companion paper also quantifies the impacts of meteorology on the aerosol-cloud relationships using numerous meteorological regimes based on lower tropospheric stability and free tropospheric relative humidity. These regimes are used for comparison with the global aerosol-climate model ECHAM6-HAM2. Also, the new CAPA diagnostics are used to select aerosols that are located far from clouds thereby providing a more consistent comparison to the GCM which simulates interactions using dry-mode aerosols. The influence of dry-mode aerosols are also found to produce a much smaller indirect forcing estimate due to the dry aerosol being a better proxy for cloud condensation nuclei. These aspects are developed and explored further in Neubauer et al. (2017).

8 Code availability

9 Data availability

The Centre for Environmental Data Analysis (CEDA; http://www.ceda.ac.uk) provided the ATSR satellite data. NASA Goddard (https://ladsweb.nascom.nasa.gov) provided the MODIS satellite data used in this paper.

Author contributions. Matthew Christensen developed the CAPA algorithm and applied it to the satellite data sets for the analysis in this paper. David Neubauer had the original idea for and helped in the design of the CAPA algorithm. Caroline Poulsen produced the AATSR-ORAC cloud products, Gareth Thomas produced the AATSR-ORAC aerosol products. Greg McGarragh, Adam Povey, Simon Proud and Don Grainger provided support needed to run ORAC. Matthew Christensen wrote the paper with comments from all co-authors.

Competing interests. The authors declare that they have no conflict of interest

Acknowledgements. We would like to thank our international members of the ORAC team at Deutscher Wetterdienst, for all of the support in running the retrieval algorithm. CEDA provided the computational infrastructure of JASMIN-CEMS needed to process this data. This research was completed as part of ERACE (The Environmental Response to Aerosols Observed in CCI ECVs), being a program of, and funded by, the European Space Agency through a Living Planet Fellowship and the Cloud_cci (contract: 4000109870/13/I-NB) and the Aerosol_cci projects (ESA Contract No. 4000109874/14/I-NB). This study was also funded as part of NERC?s support of the National Centre for Earth Observation.

References

Albrecht, B. A.: Aerosols, cloud microphysics, and fractional cloudiness, Science, 245, 1227–1230, 1989.

Amiri-Farahani, A., Allen, R. J., Neubauer, D., and Lohmann, U.: Impact of Saharan dust on North Atlantic marine stratocumulus clouds: Importance of the semi-direct effect, Atmospheric Chemistry and Physics Discussions, 2016, 1–25, doi:10.5194/acp-2016-933, http://www.atmos-chem-phys-discuss.net/acp-2016-933/, 2016.

Anderson, T. L., Charlson, R. J., Winker, D. M., Ogren, J. A., and Holmén, K.: Mesoscale Variations of Tropospheric Aerosols, Journal of the Atmospheric Sciences, 60, 119–136, doi:10.1175/1520-0469(2003)060<0119:MVOTA>2.0.CO;2, 2003.

Baum, B., Menzel, W. P., Frey, R. A., Tobin, D. C., Holz, R. E., Ackerman, S. A., Heidinger, A. K., and Yang, P.: MODIS Cloud-Top Property Refinements for Collection 6, J. Appl. Meteorol. and Clima., 51, 1145–1163, doi:10.1175/JAMC-D-11-0203.1, 2012.

Bellouin, N., Quaas, J., Morcrette, J.-J., and Boucher, O.: Estimates of aerosol radiative forcing from the MACC re-analysis, Atmospheric Chemistry and Physics, 13, 2045–2062, doi:10.5194/acp-13-2045-2013, 2013.

Benedetti, A., Morcrette, J.-J., Boucher, O., Dethof, A., Engelen, R. J., Fisher, M., Flentje, H., Huneeus, N., Jones, L., Kaiser, J. W., Kinne, S., Mangold, A., Razinger, M., Simmons, A. J., and Suttie, M.: Aerosol analysis and forecast in the European Centre for Medium-Range Weather Forecasts Integrated Forecast System: 2. Data assimilation, Journal of Geophysical Research: Atmospheres, 114, doi:10.1029/2008JD011115, d13205, 2009.

Chand, D., Wood, R., Ghan, S. J., Wang, M., Ovchinnikov, M., Rasch, P. J., Miller, S., Schichtel, B., and Moore, T.: Aerosol optical depth increase in partly cloudy conditions, Journal of Geophysical Research: Atmospheres, 117, n/a–n/a, doi:10.1029/2012JD017894, d17207, 2012.

Chen, Y.-C., Christensen, M. W., Stephens, G. L., and Seinfeld, J. H.: Satellite-based estimate of global aerosol-cloud radiative forcing by marine warm clouds, Nature Geosci, 7, 643–646, doi:10.1038/ngeo2214, 2014.

Christensen, M. W., Chen, Y.-C., and Stephens, G. L.: Aerosol indirect effect dictated by liquid clouds, Journal of Geophysical Research: Atmospheres, 121, 14,636–14,650, doi:10.1002/2016JD025245, 2016JD025245, 2016a.

Christensen, M. W., Poulsen, C., McGarragh, G., and Grainger, R. G.: Algorithm Theoretical Basis Document (ATBD) of the Community Code for CLimate (CC4CL) Broadband Radiative Flux Retrieval (CC4CL-TOAFLUX) module, ESA Cloud CCI, 1, http://www.esa-cloud-cci.org, 2016b.

Coakley, J.: A Study of Climate Sensitivity Using a Simple Energy Balance Model, Journal of the Atmospheric Sciences, 36, 260–269, doi:10.1175/1520-0469(1979)036<0260:ASOCSU>2.0.CO;2, 1979.

Feingold, G., McComiskey, A., Yamaguchi, T., Johnson, J. S., Carslaw, K. S., and Schmidt, K. S.: New approaches to quantifying aerosol influence on the cloud radiative effect, Proceedings of the National Academy of Sciences, 113, 5812–5819, doi:10.1073/pnas.1514035112, 2016.

Grandey, B. S. and Stier, P.: A critical look at spatial scale choices in satellite-based aerosol indirect effect studies, Atmospheric Chemistry and Physics, 10, 11 459–11 470, doi:10.5194/acp-10-11459-2010, 2010.

Grandey, B. S., Stier, P., and Wagner, T. M.: Investigating relationships between aerosol optical depth and cloud fraction using satellite, aerosol reanalysis and general circulation model data, Atmospheric Chemistry and Physics, 13, 3177–3184, doi:10.5194/acp-13-3177-2013, 2013.

Gryspeerdt, E., Stier, P., and Grandey, B. S.: Cloud fraction mediates the aerosol optical depth-cloud top height relationship, Geophysical Research Letters, 41, 3622–3627, doi:10.1002/2014GL059524, 2014.

Gryspeerdt, E., Stier, P., White, B. A., and Kipling, Z.: Wet scavenging limits the detection of aerosol effects on precipitation, Atmos. Chem. Phys, 15, 7557–7570, doi:doi:10.5194/acp-15-7557-2015, 2015.

Gryspeerdt, E., Quaas, J., and Bellouin, N.: Constraining the aerosol influence on cloud fraction, Journal of Geophysical Research: Atmospheres, 121, 3566–3583, doi:10.1002/2015JD023744, 2015JD023744, 2016.

Henderson, D. S., L'Ecuyer, T., Stephens, G., Partain, P., and Sekiguchi, M.: A Multisensor Perspective on the Radiative Impacts of Clouds and Aerosols, Journal of Applied Meteorology and Climatology, 52, 853–871, doi:10.1175/JAMC-D-12-025.1, 2013.

Hollmann, R.: ESA Cloud cci Product Validation and Intercomparison Report (PVIR), ESA Cloud cci, 4, xx–xx, 2017.

IPCC: Summary for policymakers, in Climate Change 2013: The Physical Science Basis, Contribution of Working Group I to the Fifth Assessment Report of the Intergovernmental Panel on Climate Change, [T. F. Stocker, D. Qin, and G. Plattner (eds.)], Cambridge University Press, Cambridge, United Kingdom and New York, NY, USA., 2013.

Lebsock, M. D., Stephens, G. L., and Kummerow, C.: Multisensor satellite observations of aerosol effects on warm clouds, J. Geophys. Res., 113, D15 205, doi:10.1029/2008JD009876, 2008.

Levy, R. C., Mattoo, S., Munchak, L. A., Remer, L. A., Sayer, A. M., Patadia, F., and Hsu, N. C.: The Collection 6 MODIS aerosol products over land and ocean, J. Atmos. Meas. Tech, 6, 2989–3032, doi:10.5194/amt-6-2989-2013, 2013.

McGarragh, G., Poulsen, C., G. Thomas, A. P., Sus, O., Schlundt, C., Stapelberg, S., Proud, S., Christensen, M., Stengel, M., and Grainger, R.: The Community Cloud Retrieval for Climate (CC4CL). Part II: The optimal estimation approach. 2017., Atmospheric Measurement Techniques, N/A, N/A, doi:In progress. To be submitted, N/A, 2017.

Morcrette, J.-J., Boucher, O., Jones, L., Salmond, D., Bechtold, P., Beljaars, A., Benedetti, A., Bonet, A., Kaiser, J. W., Razinger, M., Schulz, M., Serrar, S., Simmons, A. J., Sofiev, M., Suttie, M., Tompkins, A. M., and Untch, A.: Aerosol analysis and forecast in the European Centre for Medium-Range Weather Forecasts Integrated Forecast System: Forward modeling, Journal of Geophysical Research: Atmospheres, 114, doi:10.1029/2008JD011235, d06206, 2009.

Nakajima, T., Higurashi, A., Kawamoto, K., and Penner, J. E.: A possible correlation between satellite-derived cloud and aerosol microphysical parameters, Geophysical Research Letters, 28, 1171–1174, doi:10.1029/2000GL012186, 2001.

Neubauer, D., Christensen, M., Poulsen, C., and Lohmann, U.: Minimizing the effects of aerosol swelling and wet scavenging in the assessment of aerosol-cloud interactions, Atmospheric Chemistry and Physics, submitted, 2017.

Platnick, S. and Twomey, S.: Determining the Susceptibility of Cloud Albedo to Changes in Droplet Concentration with the Advanced Very High Resolution Radiometer, Journal of Applied Meteorology, 33, 334–347, doi:10.1175/1520-0450(1994)033<0334:DTSOCA>2.0.CO;2, 1994.

Poulsen, C. A., Watts, P. D., Thomas, G. E., and Arnold, C.: Cloud retrievals from satellite data using optimal estimation: evaluation and application to ATSR, Atmos. Meas. Tech. Discuss., 4, 2389–2431, doi:10.5194/amtd-4-2389-2011, 2012.

Quaas, J., Boucher, O., Bellouin, N., and Kinne, S.: Satellite-based estimate of the direct and indirect aerosol climate forcing, J. Geophys. Res., 113, D05 204, doi:10.1029/2007JD008962, 2008.

Quaas, J., Boucher, O., Bellouin, N., and Kinne, S.: Interpreting the cloud cover-aerosol optical depth relationship found in satellite data using a general circulation model, Atmos. Chem. Phys., 10, 6129–6135, doi:10.5194/acp-9-8697-2009, 2010.

Remer, L. A., Kaufman, Y. J., Tanré, D., Mattoo, S., Chu, D. A., Martins, J. V., Li, R.-R., Ichoku, C., Levy, R. C., Kleidman, R. G., Eck, T. F., Vermote, E., and Holben, B. N.: The MODIS Aerosol Algorithm, Products, and Validation, Journal of the Atmospheric Sciences, 62, 947–973, doi:10.1175/JAS3385.1, 2005.

Sekiguchi, M., Nakajima, T., Suzuki, K., Kawamoto, K., Higurashi, A., Rosenfeld, D., I.Sano, and Mukai, S.: A study of the direct and indirect effects of aerosols using global satellite data sets of aerosol and cloud parameters, J. Geophys. Res., 108(D22), 4699,doi:10.1029/2002JD003359, 2003.

Stephens, G., Li, J., Wild, M., Clayson, C., Loeb, N., Kato, S., L'Ecuyer, T., Stackhouse, P., Lebsock, M., and Andrews, T.: An update on Earth's energy balance in light of the latest global observations, Nature Geoscience, 5, 691–696, dOI: 10.1038/NGEO1580, 2012.

Stephens, G. L., Gabriel, P. M., and Partain, P. T.: Parameterization of Atmospheric Radiative Transfer. Part I: Validity of Simple Models, Journal of the Atmospheric Sciences, 58, 3391–3409, doi:10.1175/1520-0469(2001)058<3391:POARTP>2.0.CO;2, 2001.

Stevens, B. and Feingold, G.: Untangling aerosol effects on clouds and precipitation in a buffered system, Nature, 461, 607–613, doi:10.1038/nature08281, 2009.

Stier, P.: Limitations of passive remote sensing to constrain global cloud condensation nuclei, Atmospheric Chemistry and Physics, 16, 6595–6607, doi:10.5194/acp-16-6595-2016, 2016.

Sus, O., Jerg, M., Poulsen, C., Thomas, G., Stapelberg, S., Mcgarragh, G., Povey, A., Schlundt, C., Stengel, M., and Hollmann., R.: The Community Cloud Retrieval for Climate (CC4CL). Part I: A framework applied to multiple satellite imaging sensors., Atmospheric Measurement Techniques, N/A, N/A, in progress. To be submitted, 2017.

Ten Hoeve, J. E. and Augustine, J. A.: Aerosol effects on cloud cover as evidenced by ground-based and space-based observations at five rural sites in the United States, Geophysical Research Letters, 43, 793–801, doi:10.1002/2015GL066873, 2015GL066873, 2016.

Thomas, G. E., Carboni, E., Sayer, A. M., Poulsen, A., Siddans, R., and Grainger, R. G.: Satellite Aerosol Remote Sensing over Land: Oxford-RAL Aerosol and Cloud (ORAC): aerosol retrievals from satellite radiometers [editors Kokhanovsky, A. A. and de Leeuw, G.], Springer Berlin Heidelberg, 2009.

Twohy, C. H., Coakley, J. A., and Tahnk, W. R.: Effect of changes in relative humidity on aerosol scattering near clouds, Journal of Geophysical Research: Atmospheres, 114, n/a–n/a, doi:10.1029/2008JD010991, d05205, 2009.

Twomey, S.: Pollution and the planetary albedo, Atmos. Environ., 8, 1251–1256, 1974.

Varnái, T. and Marshak, A.: MODIS observations of enhanced clear sky reflectance near clouds, Geophysical Research Letters, 36, n/a–n/a, doi:10.1029/2008GL037089, l06807, 2009.

Várnai, T. and Marshak, A.: Analysis of co-located MODIS and CALIPSO observations near clouds, Atmospheric Measurement Techniques, 5, 389–396, doi:10.5194/amt-5-389-2012, 2012.

Várnai, T. and Marshak, A.: Effect of Cloud Fraction on Near-Cloud Aerosol Behavior in the MODIS Atmospheric Correction Ocean Color Product, Remote Sens., 7, 5283–5299, doi:10.3390/rs70505283, 2015.

Várnai, T., Marshak, A., and Yang, W.: Multi-satellite aerosol observations in the vicinity of clouds, Atmospheric Chemistry and Physics, 13, 3899–3908, doi:10.5194/acp-13-3899-2013, 2013.

Atmos. Chem. Phys. Discuss., doi:10.5194/acp-2017-450, 2017
Manuscript under review for journal Atmos. Chem. Phys.
Discussion started: 19 May 2017

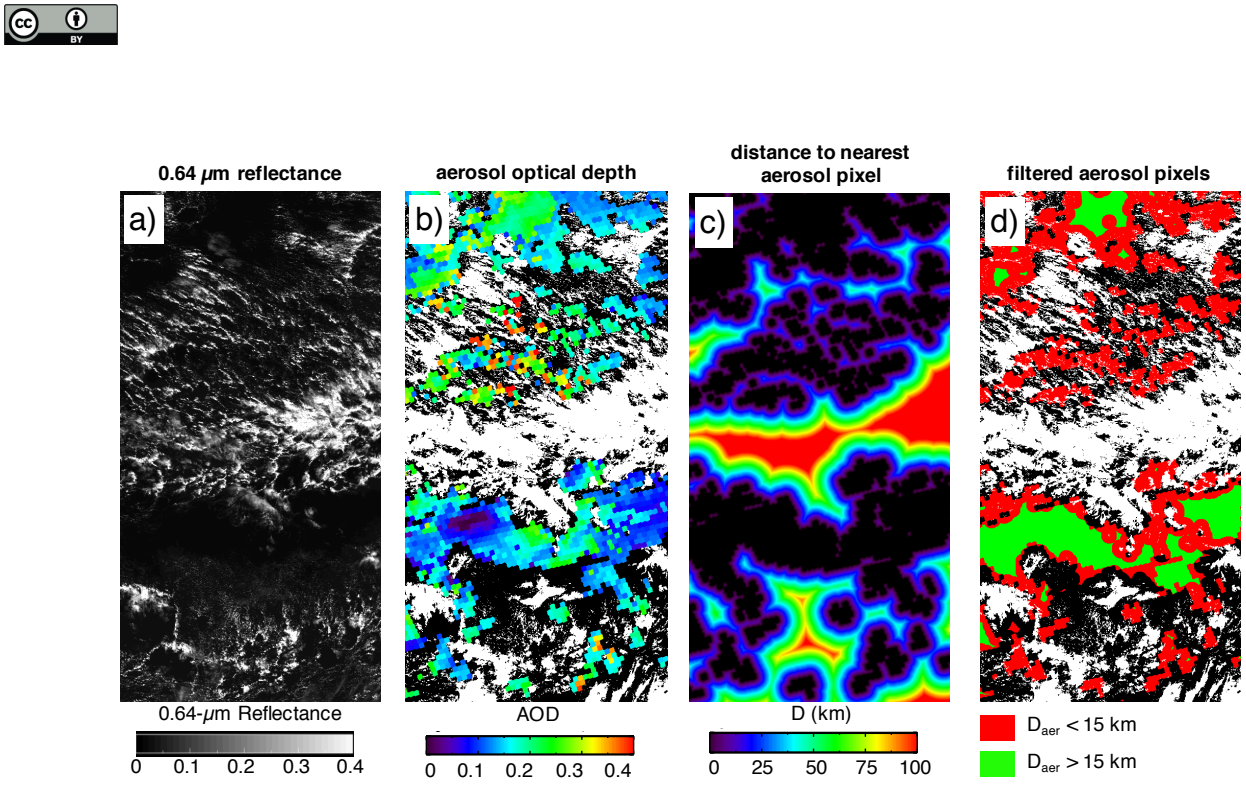

Figure 1. a) Satellite image of the visible reflectance at 0.64 μm from part of an AATSR orbit (512 ×1000 km) on the 20 June 2008 over the ocean off the west coast of Africa. b) Coinciding cloud mask (white) and aerosol optical depth (rainbow) retrieved using ORAC and c) distance from each pixel to the nearest aerosol retrieval. d) Aerosol retrievals that are located within 15 km of a cloud are considered contaminated (red) while those farther away than this are considered valid (green).

Atmos. Chem. Phys. Discuss., doi:10.5194/acp-2017-450, 2017
Manuscript under review for journal Atmos. Chem. Phys.
Discussion started: 19 May 2017

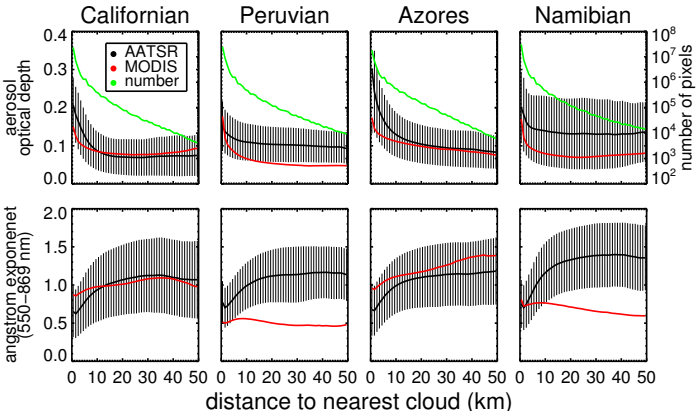

Figure 2. Mean aerosol optical depth as a function of the distance to the nearest cloud mask averaged over 1-km width bins. Relationships are plotted using AATSR-ORAC (black) and collection 6 MOD04 applied to MODIS-ORAC (red) for JJA 2008 data grouped into $10^\circ \times 10^\circ$ regions off the coasts of California ($20^\circ - 30^\circ$N, $140^\circ - 130^\circ$W), Peru ($10^\circ - 20^\circ$S, $80^\circ - 90^\circ$W), Azores ($15^\circ - 25^\circ$N, $25^\circ - 35^\circ$W), and Namibia ($10^\circ - 20^\circ$S, $0^\circ - 10^\circ$E). The number of AATSR pixels in each bin are plotted over the results (green). Error bars are denoted by the 1 standard deviation computed over the collection of AATSR retrievals within the bin.

Atmos. Chem. Phys. Discuss., doi:10.5194/acp-2017-450, 2017
Manuscript under review for journal Atmos. Chem. Phys.
Discussion started: 19 May 2017

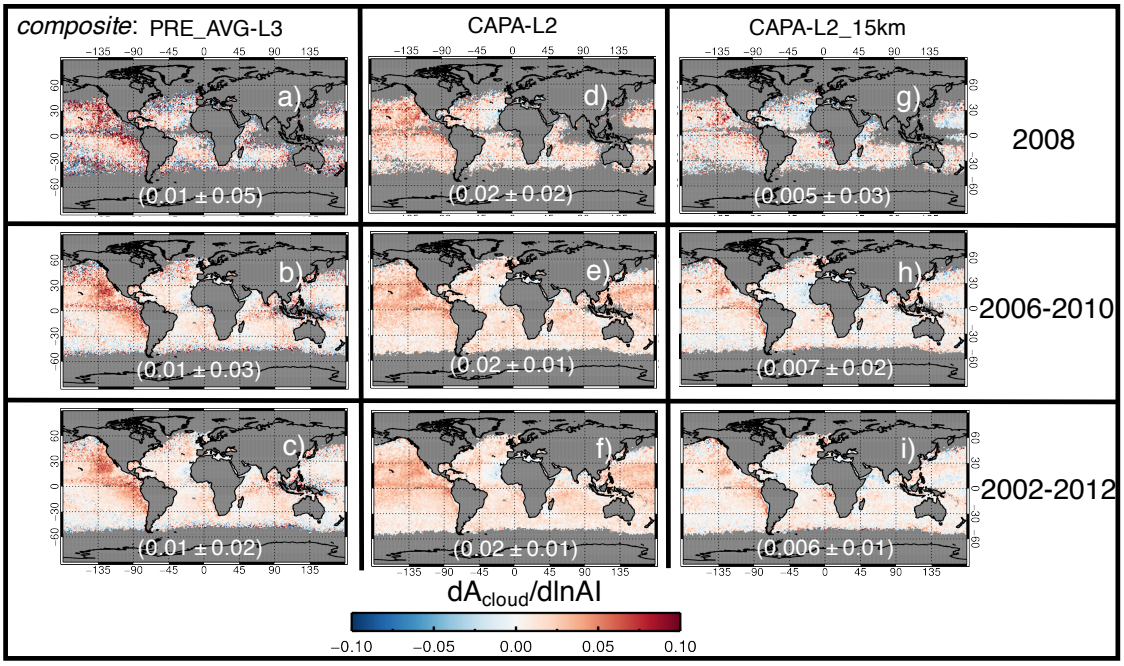

Figure 3. Cloud albedo sensitivity to changes in aerosol index averaged over $1^\circ \times 1^\circ$ regions using AATSR. Columns correspond to composites of the data based on the method selection in which the data is pre-averaged (a,b,c) using level 3 daily gridded regions (left column; Level 3), paired to the nearest high-resolution aerosol retrieval (d,e,f), and paired to nearest high-resolution aerosol retrieval that is at least 15 km away from a cloud (g,h,i). Paired observations are grouped into JJA periods using 1-year for 2008 (a,d,g), 5-years from 2006-2010, and 10 years from 2002-2012. Mean values and standard deviations are provided in parenthesis for each plot.

Atmos. Chem. Phys. Discuss., doi:10.5194/acp-2017-450, 2017
Manuscript under review for journal Atmos. Chem. Phys.
Discussion started: 19 May 2017

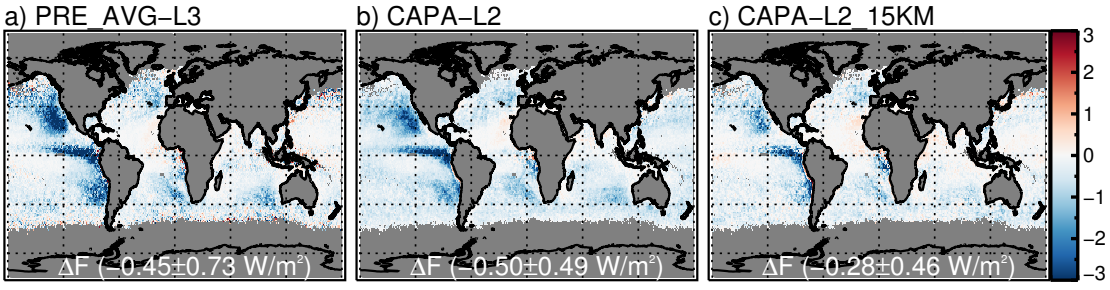

Figure 4. Intrinsic aerosol indirect radiative forcing computed using AATSR observations over oceanic $1^\circ \times 1^\circ$ regions during the period $2002 - 2012$. Oceanic mean and standard deviation of the forcing (ΔF) is given in parenthesis.

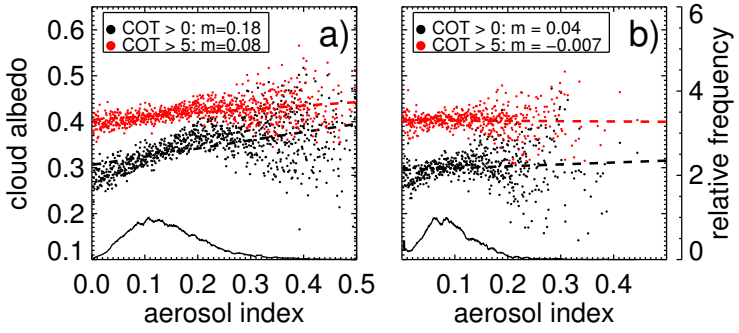

Figure 5. Binned cloud albedo as a function of aerosol index based on high-resolution aerosols that are paired to a) the nearest cloud observation (CAPA-L2 method) and b) the nearest cloud observation that is at least 15 km away (CAPA-L2_15km method) over JJA 2008. Cases are binned by 0.001 wide bins in AI over the California region ($20^\circ - 30^\circ$N, $140^\circ - 130^\circ$W) and distribution of the relative frequencies over each bin for AI are plotted over the results. Both methods are composited further by selecting cloud retrievals with cloud optical thickness (COT) greater than 5 (red points). Relative frequency of the number of cloud-aerosol occurrence is plotted beneath the scatter plot. Least squares fit line and value of the slope is provided for each composite.

Atmos. Chem. Phys. Discuss., doi:10.5194/acp-2017-450, 2017
Manuscript under review for journal Atmos. Chem. Phys.
Discussion started: 19 May 2017

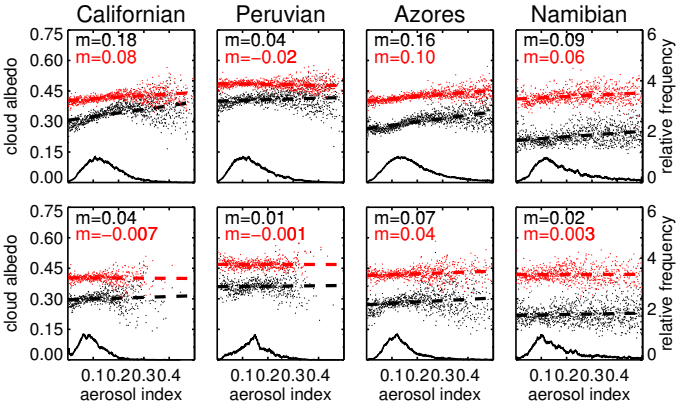

Figure 6. Same as Figure 5 but for additional regions including Peru ($10^\circ - 20^\circ$S, $80^\circ - 90^\circ$W), Azores ($15^\circ - 25^\circ$N, $25^\circ - 35^\circ$W), and Namibia ($10^\circ - 20^\circ$S, $0^\circ - 10^\circ$E).

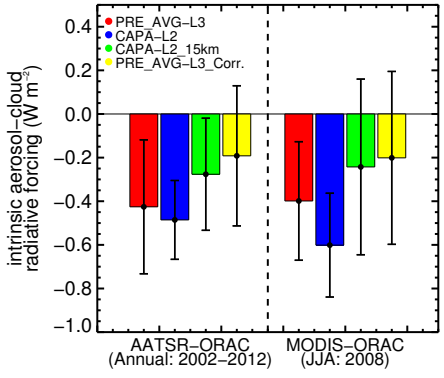

Figure 7. Estimated intrinsic aerosol-cloud radiative forcing (as defined in equation 4) by global marine warm clouds derived using top of atmosphere shortwave fluxes from AATSR-ORAC (left columns) and MODIS-ORAC (right columns). Estimates are provided using the pre-average standard level-3 products (PRE_AVG-L3 composite; red), and pre-average corrected level-3 products in which the nearest aerosol is located at least 15 km from any other cloud (PRE_AVG-L3_Corr.; yellow), cloud pairs using the nearest high-resolution aerosol retrieval (CAPA-L2; blue), cloud pairs using the nearest high-resolution aerosol retrieval that is at least 15 km away from any other cloud (CAPA-L2_15km; blue). Error bars are calculated on the basis of the standard error of the regression slope.

Atmos. Chem. Phys. Discuss., doi:10.5194/acp-2017-450, 2017
Manuscript under review for journal Atmos. Chem. Phys.
Discussion started: 19 May 2017

Atmospheric Chemistry and Physics Discussions

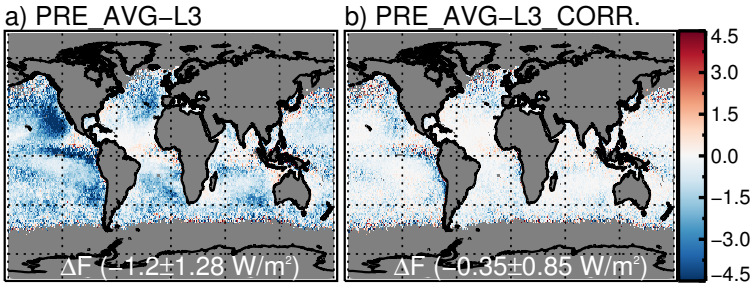

Figure 8. Extrinsic aerosol indirect radiative forcing computed using AATSR observations over oceanic $1^\circ \times 1^\circ$ regions during the period $2002 - 2012$. Oceanic mean and standard deviation of the forcing (ΔF) is given in parenthesis.

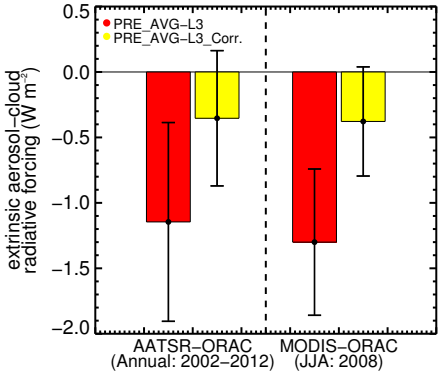

Figure 9. Estimated extrinsic aerosol-cloud radiative forcing (as defined in equation 4) by global marine warm clouds derived using top of atmosphere shortwave fluxes from AATSR-ORAC (left columns) and MODIS-ORAC (right columns). Estimates are provided using the pre-average standard level-3 products (PRE_AVG-L3 composite; red), and pre-average corrected level-3 products in which the nearest aerosol is located at least 15 km from any other cloud (PRE_AVG-L3_Corr.; yellow). Error bars are calculated on the basis of the standard error of the regression slope.

Atmos. Chem. Phys. Discuss., doi:10.5194/acp-2017-450, 2017
Manuscript under review for journal Atmos. Chem. Phys.
Discussion started: 19 May 2017

Atmospheric Chemistry and Physics Discussions

Table 1. Summary of composites used in this study

Composite	Description
Nearest high-resolution cloud-aerosol pair (CAPA-L2)	Comprised of level-2 individual pairs of pixels in which the length-scale between the cloud and nearest high-resolution aerosol retrieval can range from 0 to 150 km. An example of the pixel selection for these cases is displayed in Figure 1d; green pixels.
Nearest high-resolution cloud-aerosol pair separated by at least 15 km (CAPA-L2_15km)	Same as above except the nearest high-resolution aerosol retrieval has to be located at least 15 km from any other cloud and cannot exceed a pairing length-scale beyond 150 km. An example of the pixel selection for these cases is displayed in Figure 1d; red pixels.
Pre-averaged cloud & aerosol (PRE_AVG-L3)	Pairs are based on un-colocated level-3 pre-averaged $1^\circ \times 1^\circ$ cloud and aerosol observations from standard MODIS (i.e. MOD08) and AATSR products.
Pre-averaged cloud & corrected aerosol (PRE_AVG-L3_Corr.)	Same as above except the cloud observations are paired to a new aerosol dataset based on pre-averaging only those aerosol pixels that are located at least 15 km away from cloud.

Atmos. Chem. Phys. Discuss., doi:10.5194/acp-2017-450, 2017
Manuscript under review for journal Atmos. Chem. Phys.
Discussion started: 19 May 2017

Atmospheric Chemistry and Physics Discussions

Table 2. Aerosol-cloud radiative forcing estimated using equation 4 based on ORAC applied to AATSR over the $2002-2012$ period and ORAC applied to MODIS collection 6 observations over JJA-2008 for low-level warm maritime clouds. Uncertainties are calculated on the basis of the propagated standard error of the regression slope through the radiative forcing calculation.

	Intrinsic Forcing (W m^{-2})		Extrinsic Forcing (W m^{-2})	
	AATSR	MODIS	AATSR	MODIS
Nearest high-resolution cloud-aerosol pairs (CAPA-L2)	-0.49 ± 0.18	-0.60 ± 0.24	N/A	N/A
Nearest high-resolution cloud-aerosol pairs aerosol is at least 15 km from any cloud (CAPA-L2_15km)	-0.28 ± 0.26	-0.24 ± 0.40	N/A	N/A
Pre-averaged 1° cloud & aerosol pairs (PRE_AVG-L3)	-0.43 ± 0.31	-0.40 ± 0.27	-1.1 ± 0.76	-1.3 ± 0.56
Pre-averaged 1° cloud & corrected aerosol pairs pre-averaged aerosols are at least 15 km from clouds (PRE_AVG-L3_Corr.)	-0.19 ± 0.32	-0.20 ± 0.40	-0.35 ± 0.52	-0.38 ± 0.42